Research Square

Preprints are preliminary reports that have not undergone peer review.
They should not be considered conclusive, used to inform clinical practice,
or referenced by the media as validated information.

How one brain substrate generates many ideas. A Geometro-Diffusion Theory model

Ernesto Estrada

estrada@ifisc.uib-csic.es

Institute for Cross-Disciplinary Physics and Complex Systems

Research Article

Keywords:

Posted Date: November 20th, 2026

DOI: https://doi.org/10.21203/rs.3.rs-11633926/v1

License: This work is licensed under a Creative Commons Attribution 4.0 International License.
Read Full License

Additional Declarations: No competing interests reported.

How one brain substrate generates many ideas. A Geometro-Diffusion Theory model

Ernesto Estrada[1*]

[1*]Institute for Cross-Disciplinary Physics and Complex Systems (IFISC, UIB-CSIC), Palma de Mallorca, Spain.

Corresponding author(s). E-mail(s): estrada@ifisc.uib-csic.es;

Abstract

A brain has one anatomical network and one set of physiological laws, yet it holds a very large number of different ideas. We propose a mechanism for this variety within the Geometro-Diffusion Theory (GDT) of consciousness, which associates experience with the geometry generated by propagation across the brain. In the model, every input induces, at the time at which the geometry is read, an effective network: the regions whose activity is, or has been, above a threshold. Each effective network carries its own part of the brain's geometry and corresponds to one idea, which a reader, the diffusion-based machine, reads and associates with what is felt. The dynamics derives from the dynamic mean-field model of the cortex. On the human connectome, tens of thousands of inputs produce tens of thousands of different effective networks, the same network is reached from different inputs, and geometric richness varies widely. Along the coupling axis fitted to anaesthesia and psychedelic data, the networks become poorer at loss of responsiveness and richer under psilocybin. The picture and the name of an item produce different networks, which the reader associates after learning both. Having learned the propagation from short repeated episodes, the reader reads the geometry of every effective network immediately. With two images present, both networks are generated and a serial reader reads them in turn, weighted by richness and familiarity, as in binocular rivalry. Finally, the predicted networks overlap the cortical parcels that respond to electrical stimulation in 780 patients, well above chance.

Keywords: consciousness, diffusion geometry, effective networks, connectome, dynamic mean-field model, cortico-cortical evoked potentials

1 Introduction

A theory of consciousness must explain not only why a brain is conscious but also how the same brain holds many different contents: the redness of a rose, the face of a friend, the sound of a word. The anatomical network of a given brain is fixed on the time scale of an experience, and so are the physiological laws that govern the propagation of activity on it. Whatever generates the variety of conscious contents must therefore be found in the activity that this fixed substrate supports. The question addressed in this paper is how one substrate and one dynamics give rise to many ideas, and how each of them is made available to the brain that holds it.

The main theories of consciousness approach this question in different ways (Seth and Bayne, 2022; Storm et al., 2024). Integrated information theory (IIT) identifies an experience with the cause–effect structure specified by a system in its current state (Oizumi et al., 2014; Tononi et al., 2016). Different contents correspond to different states, and the similarity of two experiences is in principle the distance between their structures in a "quality space". The strength of IIT in this respect is that it identifies content with a structure and not with a single signal; its weakness is that the structure is not computable for a real brain, so the repertoire of contents and the relations between them cannot be evaluated, and the theory gives no mechanism by which one content is reached from an input (Kleiner and Tull, 2021; Tononi et al., 2025). Global neuronal workspace theory relates conscious access to the broadcasting of a local representation to the whole brain through ignition (Dehaene and Changeux, 2011; Mashour et al., 2020). Its strength is a clear mechanism of access, supported by imaging and electrophysiology; content, however, is assigned to the specialized processors whose representation is broadcast, so that the variety of contents is inherited from those processors and is not explained by the workspace itself. Higher-order theories place content in the higher-order representation of a first-order state (Brown et al., 2019). They explain how a perceived and an imagined content can be the same, since the higher-order representation can be shared, but they say little about how the repertoire of first-order states is generated. Predictive processing describes perception as inference under a generative model, and imagery as the same model run without sensory input (Hohwy and Seth, 2020; Friston, 2018). It offers a natural account of shared content across perception and imagery, but the content is a hypothesis of the model, and the relation between the model and the propagation of activity on the anatomical network is not specified. Recurrent processing theory associates conscious perception with recurrent interactions in sensory cortex (Lamme, 2006), and the entropic-brain hypothesis and coordination-dynamics accounts relate the richness of experience to the entropy and the metastability of brain dynamics (Carhart-Harris et al., 2014; Schartner et al., 2017; Shanahan, 2010; Deco et al., 2017); these accounts address the level and the richness of consciousness more than the identity of its contents. In every case, the step from the activity on a fixed anatomical network to a specific content, and to the many contents of one brain, remains qualitative.

Two experimental observations constrain any answer. First, single neurons of the human medial temporal lobe respond to one person or object whether it is presented as different pictures or as its written or spoken name (Quian Quiroga et al., 2005, 2009; Quian Quiroga, 2012); the same content is therefore reached from inputs that

enter the brain through different systems. Second, imagery reactivates sensory cortex, with activity patterns that overlap only partly with those of perception (Dijkstra et al., 2019). Contents are thus carried by patterns of activity distributed over many regions (Haxby et al., 2001; Haynes and Rees, 2006), and the same content can be reached from different patterns.

The Geometro-Diffusion Theory (GDT) associates conscious experience with the geometry generated by the propagation of activity on the anatomical network and read by the brain's own recurrent circuits (Estrada, 2027, 2026d,c,b). In its formulation so far, one substrate and one dynamics generate one geometry. This geometry follows the conscious state: it collapses at loss of consciousness in models of anaesthesia (Estrada, 2026d), and on the human connectome it decreases at loss of responsiveness under propofol and increases under psilocybin, while remaining nearly unchanged under a magnetic field that leaves the conscious state intact (Estrada, 2026a). A single geometry, however, cannot by itself account for many contents. Here we propose that the variety comes from the inputs: every input induces, at the time at which the geometry is read, its own effective network, the part of the substrate reached by the propagation, and this network carries its own part of the geometry. One idea corresponds to one effective network.

We formulate this proposal as a model, derive its dynamics from the dynamic mean-field model of the human cortex (Wong and Wang, 2006; Deco et al., 2014), and study it on the human connectome. We show that the repertoire of effective networks is very large and that the same network is reached from different inputs; that the networks are connected; that their geometric richness varies widely; that they change with the conscious state along the coupling axis fitted to anaesthesia and psychedelic data; that inputs entering through different sensory systems produce different networks, which a recurrent reader associates with the same item after learning; that a reader learns the propagation of the substrate by repetition and then reads the geometry of every effective network immediately; and that the effective networks predicted on the human connectome overlap the regions that respond to direct electrical stimulation of the human cortex (David et al., 2013; Trebaul et al., 2018).

2 The Geometro-Diffusion Theory

2.1 Observation and experience

GDT starts from a distinction between two things to which a quantity computed from brain activity can refer (Estrada, 2027, 2026b). A spectrometer directed at a ripe tomato reports that the reflected light has most of its power at long wavelengths, and a cone of the retina responds to that light with a definite change of its membrane current. Both are observations: each is a property of one signal at one place. The experience of red is of another kind: red is experienced as close to orange and to purple and far from green, and it is defined by its place among all other colours, in a space of relations. GDT makes the same distinction for the brain. When one region is perturbed, the activity that propagates from it to all other regions is a single response, an observation. When every region is perturbed in turn, the responses define distances between regions, the distances between the ways in which activity propagates from

them. These distances form a geometry, and it is this geometry, a structure of relations generated by all responses together, that GDT associates with conscious experience.

2.2 The geometry

Let $P(t)$ be the propagator of a linear dynamics on the anatomical network, so that $P_{ij}(t)$ is the activity of region i at time t after a unit perturbation of region j. The diffusion distance between regions i and j is

$$D_{ij}^2(t) = P_{ii}(t) + P_{jj}(t) - 2P_{ij}(t),$$

which, for a symmetric propagator, is the squared Euclidean distance between the responses $P(t/2)\boldsymbol{e}_i$ and $P(t/2)\boldsymbol{e}_j$ to the two perturbations (Coifman and Lafon, 2006; Estrada, 2027). The regions are then the vertices of a simplex whose edge lengths are the diffusion distances, and this simplex is the geometry of the substrate at time t.

2.3 Differentiation and its time course

The differentiation of the geometry is measured by the signature information,

$$I_{\mathrm{sig}}(t) = \frac{2}{n} \sum_{i=1}^{n} \sum_{k=1}^{n} \big(S_{ik}(t) - \bar{S}_k(t)\big)^2,$$

where the row $S_{i\cdot}(t)$ contains the distances from region i to all regions sorted in increasing order and $\bar{S}_k(t)$ is the mean of the k-th sorted distance over all regions (Estrada, 2027). I_{sig} is zero when all regions occupy equivalent relational positions and grows as their distance profiles become different. Immediately after a perturbation the responses are all local and the geometry is undifferentiated; at long times every response has spread over the whole network and the distances collapse. In between, $I_{\mathrm{sig}}(t)$ reaches a maximum $I_{\mathrm{sig}}^{\max}$ at a time $t_{\max}$, the time of maximal differentiation of the geometry. GDT associates a conscious state with a geometry that is strongly differentiated, with a large $I_{\mathrm{sig}}^{\max}$, and quickly, with a short $t_{\max}$ (Estrada, 2027, 2026d).

2.4 The reader: the diffusion-based machine

A geometry that is generated and not read is not an experience: a drop of milk spreading in coffee generates relations among its parts, but nothing reads them. GDT formalizes the reading with the diffusion-based machine (DBM), a recurrent network that receives the activity of the substrate and decodes the geometry from it (Estrada, 2026c). The DBM has two readouts that share the same internal states: an observational readout, which identifies the region where a perturbation entered, and a geometric readout, which recovers the coordinates of the geometry. For linear propagation, the geometry of all possible perturbations is fixed by the evolution operator, so that a reader that learns the operator from the activity it receives obtains the geometry of all responses without the family of responses ever being realized (Estrada, 2026c). The quantity that GDT associates with conscious experience is the geometry generated and read. On the human connectome, the product of $I_{\mathrm{sig}}^{\max}$ and of the

fidelity of the DBM reading follows responsiveness under propofol and the intensity of experience under psilocybin (Estrada, 2026a).

2.5 From one geometry to many ideas

With a fixed substrate and a fixed dynamics, $P(t)$ and therefore the geometry of the whole brain are fixed. The present paper adds to GDT the step from this single geometry to the many ideas that one brain holds, through the effective networks defined in the next section.

3 The model

The model has four ingredients, which Fig. 1 illustrates on a toy substrate before they are defined formally: an anatomical substrate on which activity propagates, an input that starts the propagation, the effective network that the input selects at the time at which the geometry is read, and a reader that reads the geometry of that network and associates it with what is felt.

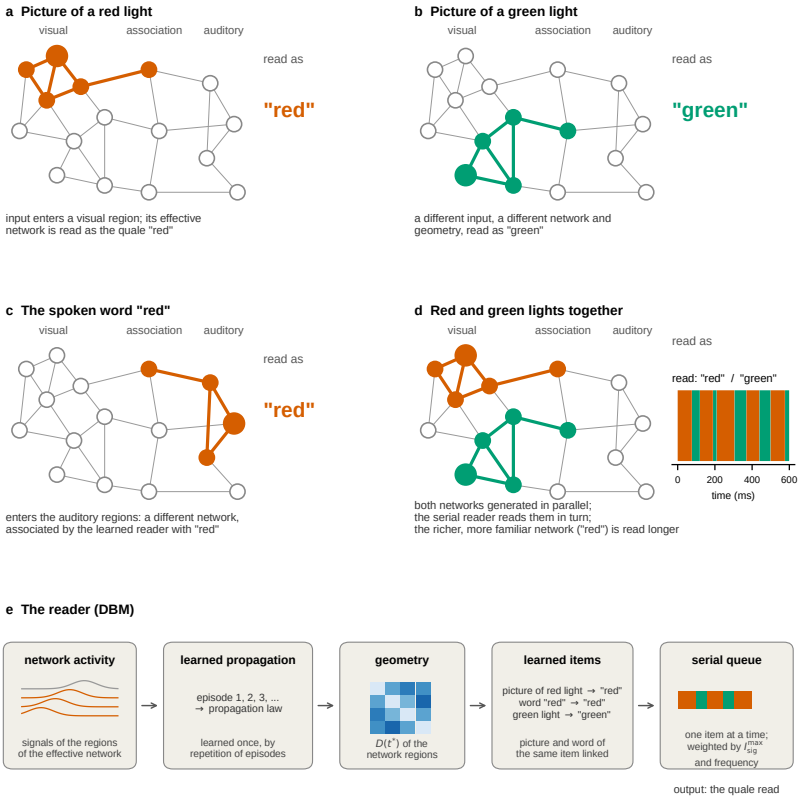


Fig. 1 From inputs to qualia: an illustration on a toy substrate with visual, association and auditory regions. **a**, The picture of a red light enters one visual region (large circle). Within the reading time t^* its activity reaches the neighbouring regions, and the regions whose activity is, or has been, above the threshold form its effective network (coloured regions and edges). The geometry of these regions is read as the quale "red". **b**, The picture of a green light enters another visual region: a different effective network, with a different geometry, read as "green". One substrate and one dynamics thus give different ideas for different inputs. **c**, The spoken word "red" enters the auditory regions and produces a third effective network, different from that of the picture; the reader, which has learned the picture and the word of the same item together, associates it with the same item. **d**, When the red and the green lights are present at once, both effective networks are generated in parallel, and the serial reader reads them in turn; the strip shows the quale read over time, with the network of richer geometry and greater familiarity (here "red") read for longer. **e**, The reader, the diffusion-based machine (DBM): it receives the activity of the regions of the effective network; it has learned the propagation law of the substrate once, by repetition of many short episodes; from this law it reads the geometry $D(t^*)$ of the active regions immediately; it associates the read geometry with learned items, linking the picture and the word of the same item; and a serial queue delivers one item at a time, weighted by the geometric richness $I_{\mathrm{sig}}^{\max}$ and the frequency of each effective network. The output is the quale read. The substrate, networks and time course are illustrative; the corresponding quantities on the human connectome are given in the Results.

3.1 Substrate and dynamics

The substrate is the human cortical connectome, a weighted undirected graph $\Gamma = (V, E)$ with n regions, weighted adjacency matrix W, strengths $d_i = \sum_j W_{ij}$ and Laplacian $L = K - W$, $K = \mathrm{diag}(d_1, \ldots, d_n)$; the toy substrate of Fig. 1a plays the same role on a small scale. The weights are normalized to unit mean strength, which fixes the units of the global coupling introduced below (Methods).

The dynamics is derived from the dynamic mean-field (DMF) model of the cortex (Wong and Wang, 2006; Deco et al., 2014), in which every region is described by an excitatory and an inhibitory population coupled to the other regions through the connectome scaled by a global coupling G. Feedback inhibition control sets the local inhibition of every region so that all regions fire at the same rate (Deco et al., 2014), which makes the inhibitory coupling of every region grow linearly with its strength. Near the stationary state, fast inhibition follows excitation adiabatically on the time scales of propagation, and the deviations $\boldsymbol{x}$ of excitatory activity from the stationary state obey

$$\dot{\boldsymbol{x}} = -M\boldsymbol{x} + \boldsymbol{\xi}(t), \qquad \boldsymbol{x}(0) = \boldsymbol{u}, \qquad M = \Lambda + \kappa L, \qquad \Lambda = \mathrm{diag}(\Lambda_1, \ldots, \Lambda_n),$$

with

$$\Lambda_i = \lambda_0 - \kappa(1 - \vartheta)\, d_i, \qquad \kappa = \kappa_0 G,$$

$\lambda_0 = 5.952\ \mathrm{s}^{-1}$, $\kappa_0 = 7.287\ \mathrm{s}^{-1}$ and $\vartheta = 0.357$, and with $\boldsymbol{\xi}$ a noise vector (Estrada, 2026a). The initial condition $\boldsymbol{u}$ is the input, the pattern of activity with which a stimulus enters the substrate, and it is this initial condition that defines the effective network below. Long-range excitation supplies activity from neighbouring regions, which gives the Laplacian term, and strength-dependent feedback inhibition provides the corresponding loss, which gives the region-dependent leak Λ_i. We call this model the coupling model. It is a diffusion model: it rewrites the DMF near its stationary state as the diffusion of activity on the connectome, through the Laplacian L with rate κ, together with a region-dependent leak Λ_i. Its propagator is

$$P(t) = e^{-tM}.$$

Because the off-diagonal entries of $-M$ are nonnegative, $P(t)$ has nonnegative entries at all times, and a nonnegative input produces nonnegative activity everywhere. The leak is positive in weakly connected regions and negative in the most strongly connected ones, which in isolation would amplify a perturbation; the network is nevertheless stable, because diffusion drains activity from these regions to their neighbours. Unless stated otherwise $G = 0.96$, the median coupling fitted to the awake state of the propofol volunteers in (Estrada, 2026a).

3.2 Reading time

The geometry is read at the time t^* at which the geometry of the whole substrate is most differentiated,

$$t^* = t_{\max} = \arg\max_t\, I_{\mathrm{sig}}(t),$$

computed from $P(t)$ of the whole substrate. On the cortical connectome used here, $t^* = 0.217$ s at the awake coupling. What happens after t^* plays no role in the model.

3.3 Effective networks

An input to the brain is represented by the nonnegative initial condition $\boldsymbol{u}$ of the dynamics, normalized to unit total mass, $\sum_i u_i = 1$, so that one threshold applies to all inputs; its activity is $\boldsymbol{x}(t) = P(t)\boldsymbol{u}$. In the example of Fig. 1a, the picture of a red light is an input concentrated on one visual region, marked by the large circle, and the activity it starts spreads from there to the neighbouring regions.

Definition 1 (effective network). Let $\theta > 0$ be a threshold. The vertex set of the effective network induced by $\boldsymbol{u}$ is the set of regions whose activity is, or has been, at least θ up to the reading time,

$$V_\theta(\boldsymbol{u}, t^*) = \Big\{ i \in V : \max_{0 \le s \le t^*} x_i(s) \ge \theta \Big\},$$

and the effective network $\Gamma_\theta(\boldsymbol{u}, t^*)$ is the subgraph of Γ induced by $V_\theta(\boldsymbol{u}, t^*)$. In Fig. 1a and b the effective networks of the red and the green light are the coloured regions and edges: two different inputs on the same substrate select two different networks.

The rule "is or has been" guarantees connectivity under the condition of the following proposition. Because diffusion behaves as a random walk, a region can reach the threshold only after one of its neighbours has reached it.

Proposition 1 (connectivity). If $\Lambda_i \ge 0$ for every region, every connected component of $\Gamma_\theta(\boldsymbol{u}, t^*)$ contains a region of the support of $\boldsymbol{u}$. In particular, if the initial condition is supported on a connected set of regions and $u_i \ge \theta$ for every region i of its support, the effective network is connected.

Proof. Let $j \in V_\theta(\boldsymbol{u}, t^*)$ with $u_j = 0$, and let $t_1 \le t^*$ be the first time at which $x_j(t_1) = \theta$. Suppose that no neighbour k of j has reached θ in $[0, t_1]$. By continuity, $m = \max_{k \sim j} \max_{0 \le s \le t_1} x_k(s) < \theta$. For $0 \le t \le t_1$, since $x_j \ge 0$ and $\Lambda_j \ge 0$,

$$\dot{x}_j = -\Lambda_j x_j + \kappa \sum_k W_{jk}(x_k - x_j) \le \kappa d_j (m - x_j),$$

and, with $x_j(0) = 0$, $x_j(t) \le m\big(1 - e^{-\kappa d_j t}\big) < \theta$, a contradiction. Hence some neighbour of j reached θ before t_1, and it belongs to $V_\theta(\boldsymbol{u}, t^*)$. Repeating the argument, with first-passage times that decrease strictly, gives a path in $\Gamma_\theta(\boldsymbol{u}, t^*)$ from j to a region of the support of $\boldsymbol{u}$. When $u_i \ge \theta$ on the support, every region of the support belongs to $V_\theta(\boldsymbol{u}, t^*)$; the support is connected, so all components are joined through it and the effective network is connected. □

In the coupling model the leak is negative in the most strongly connected regions, where the bound used in the proof does not hold; there the property is verified numerically in the Results.

Definition 2 (frequency and repertoire). Let $\mathcal{U}$ be a family of initial conditions with a probability measure μ. The frequency of an effective network Γ_e is the measure

of the set of initial conditions that produce it,

$$\phi(\Gamma_e) = \mu\big(\{\boldsymbol{u} \in \mathcal{U} :\ \Gamma_\theta(\boldsymbol{u}, t^*) = \Gamma_e\}\big),$$

estimated by the number of sampled initial conditions that produce Γ_e. The repertoire of the substrate is the set of effective networks with nonzero frequency. A red light seen in slightly different conditions, for instance, gives slightly different inputs, and when these select the same network that network is reached more often and has a higher frequency.

3.4 The geometry of an effective network

Each effective network Γ_e, with vertex set V_e, carries the geometry of the whole substrate restricted to its regions,

$$D^{(e)}_{ij}(t) = D_{ij}(t), \qquad i, j \in V_e,$$

that is, the face of the simplex of the whole substrate spanned by the regions of the effective network, shown as a small distance matrix in Fig. 1e. Its differentiation $I^{(e)}_{\mathrm{sig}}(t)$ is computed from these distances with n replaced by $|V_e|$, and its maximum $I^{\max,(e)}_{\mathrm{sig}}$ and the time $t^{(e)}_{\max}$ of that maximum characterize the geometric richness of the effective network in the same way as for the whole substrate. Given the substrate and the dynamics, the set of regions of an effective network therefore determines its geometry uniquely.

3.5 From geometry to idea

An idea is an effective network with its geometry, as read by the reader. For instance, an idea can be the redness of a traffic light: its picture selects the network of Fig. 1a, the reader reads the geometry of that network, and what is read is felt as “red”. Each presentation of an input thus gives its own effective network and its own geometry, and it is this geometry that is experienced. The identity of an item across presentations, such as the redness shared by the picture of a red light and the spoken word “red”, is of another kind: it is not carried by any single network but is an association learned by the reader. Seeing red, hearing the word “red” and recognizing that both refer to the same colour are therefore different things in the model, the first two being two geometries and the third a learned link between them. The number of different ideas that a substrate can hold is the number of different effective networks in its repertoire, and the frequency of an effective network measures how often it is reached. The reader, the DBM of Fig. 1e, learns the propagation of the substrate; once it has learned it, the input selects the effective network and the reader reads the geometry of its regions. The reader also associates what it reads with what is felt, a word, a picture or a sound. In this way the spoken word “red” of Fig. 1c, which enters through the auditory regions and produces a network different from that of the picture, is associated with the same item once the reader has learned the picture and the word together. When two incompatible inputs are present at once, as the red and the green

light of Fig. 1d, the reader reads their networks in turn. Fig. 2 shows the propagation that underlies these steps on a small graph.

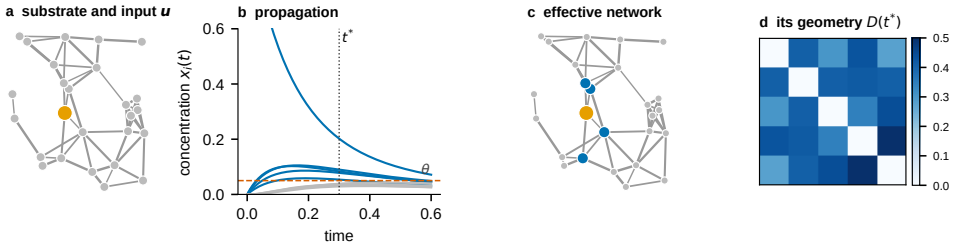


Fig. 2 Propagation and effective network on a small illustrative graph. **a**, Substrate and an input $\boldsymbol{u}$ on one region (orange). **b**, Propagation of the activity $x_i(t)$ of the regions closest to the input; blue curves, regions whose activity is or has been at least θ (dashed line) up to the reading time t^* (dotted line); grey, regions that stay below θ. **c**, The effective network: the input region and the regions in blue. **d**, Its geometry, the diffusion distances $D_{ij}(t^*)$ of the whole substrate restricted to the regions of the effective network.

4 Results

Unless stated otherwise, the substrate is the group-consensus connectome of the Schaefer-100 parcellation (Hansen et al., 2022; Schaefer et al., 2018), with 100 cortical regions and 1136 connections, at the awake coupling $G = 0.96$, with $t^* = 0.217$ s and $\theta = 0.01$. Two families of inputs are used: localized inputs, on one region and up to three of its neighbours with random amplitudes, and distributed inputs, on one to ten regions chosen anywhere with random amplitudes (Methods).

4.1 A very large repertoire of ideas

The first relevant result is that the model generates a very large repertoire of effective networks. In fact, from 15,073 different localized inputs the substrate produced 12,438 different effective networks, with a median of 23 regions, and from 18,105 different distributed inputs it produced 18,022 different effective networks. The number of different networks grew almost in proportion to the number of inputs, with 1,866, 3,509, 6,708 and 12,438 networks for 2,500, 5,000, 10,000 and 20,000 sampled localized inputs, and it showed no sign of saturation (Fig. 3a). The repertoire of the substrate is therefore much larger than any of these samples, and the same holds for the thresholds $\theta = 0.005$, 0.02 and 0.05.

It is remarkable that, within this large repertoire, different inputs often lead to exactly the same effective network, which is what happens in Fig. 1a when a red light seen in slightly different conditions selects the same set of regions. We say that an effective network is repeated when two or more different inputs produce it. Among the localized inputs, 1,441 effective networks were repeated in this sense, 956 of them by inputs that started in different sets of regions, and one network was produced

from 14 different sets of starting regions; the most frequent network was produced by 21 different inputs (Fig. 3b–d). Repeated networks are rarer among distributed inputs, where 68 networks were produced by two or more inputs and none by more than five. The frequency of an effective network (Definition 2) thus varies widely across the repertoire. For localized inputs its distribution is fitted by a power law with exponent 3.4 (discrete maximum-likelihood fit (Clauset et al., 2009)), better than by an exponential (likelihood-ratio test (Vuong, 1989), $p \approx 10^{-30}$), and an exponential cutoff does not improve the fit ($p = 0.39$); the exponents are 3.6 and 2.9 for $\theta = 0.005$ and 0.02. The frequencies span from 1 to 21, about 1.3 decades.

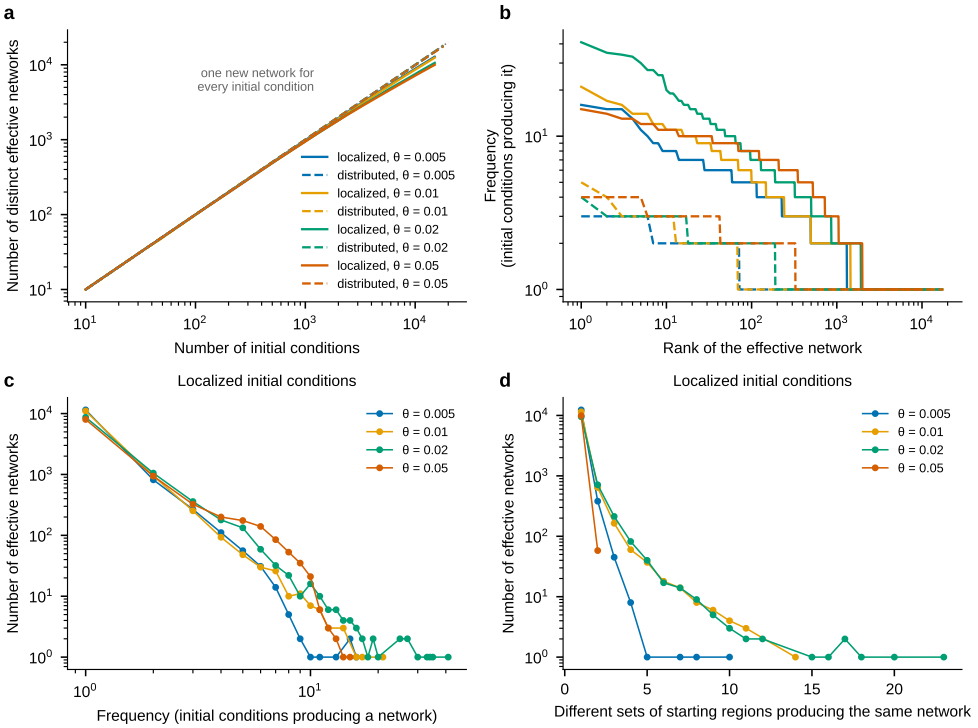


Fig. 3 Repertoire of effective networks. **a**, Number of different effective networks against the number of sampled inputs, for localized and distributed inputs and four thresholds; the dashed line marks one new network per input. **b**, Frequency of each effective network (number of inputs that produce it) against its rank. **c**, Distribution of the frequencies for localized inputs. **d**, Number of different sets of starting regions that produce the same effective network.

On the one hand, Proposition 1 guarantees that every component of an effective network contains a region where the input entered when the leak is nonnegative everywhere. On the other hand, in the coupling model the leak is negative in 15 of the 100 regions, so the property has to be checked numerically. In 3,000 inputs checked for each family, every component of every effective network contained a starting region.

Every localized input satisfies the support and initial-amplitude conditions of the corollary, since the smallest initial amplitude of a starting region, about 0.02, is above θ, and localized inputs always produced connected networks. Effective networks with several components arose from distributed inputs with distant starting regions, each component being organized around its own entry regions.

It is also worth mentioning that the ideas of the repertoire are far from equivalent in geometric richness. For every one of the 30,460 effective networks, the signature information of its geometry rises, reaches a maximum and decays, as it does for the whole substrate (Fig. 4). The time of maximal differentiation is close to that of the whole brain: 0.19–0.24 s for localized inputs (median 0.214 s) and 0.18–0.42 s for distributed inputs (median 0.221 s), the longest times appearing in networks of fewer than 15 regions. The maximal differentiation $I_{\mathrm{sig}}^{\max}$, by contrast, ranges from about 0.0001 to 0.046, while that of the whole brain is 0.093. It grows with the number of regions (Pearson correlation 0.83 for localized and 0.76 for distributed inputs), and at equal size it varies by up to a factor of four; for networks of 20 regions, for example, it goes from about 0.008 to 0.035. If we apply the criterion used for small graphs in GDT, namely $I_{\mathrm{sig}}^{\max}$ above its mean and $t_{\max}$ below its mean (Estrada, 2027), we select 2,884 of the 12,438 localized networks (23%) and 5,454 of the 18,022 distributed ones (30%). The repertoire therefore contains ideas of very different geometric richness. Interestingly, the frequency of a network is independent of its richness (Spearman correlation -0.11 for localized and 0.01 for distributed inputs), so that the ideas reached most often are not necessarily the richest ones.

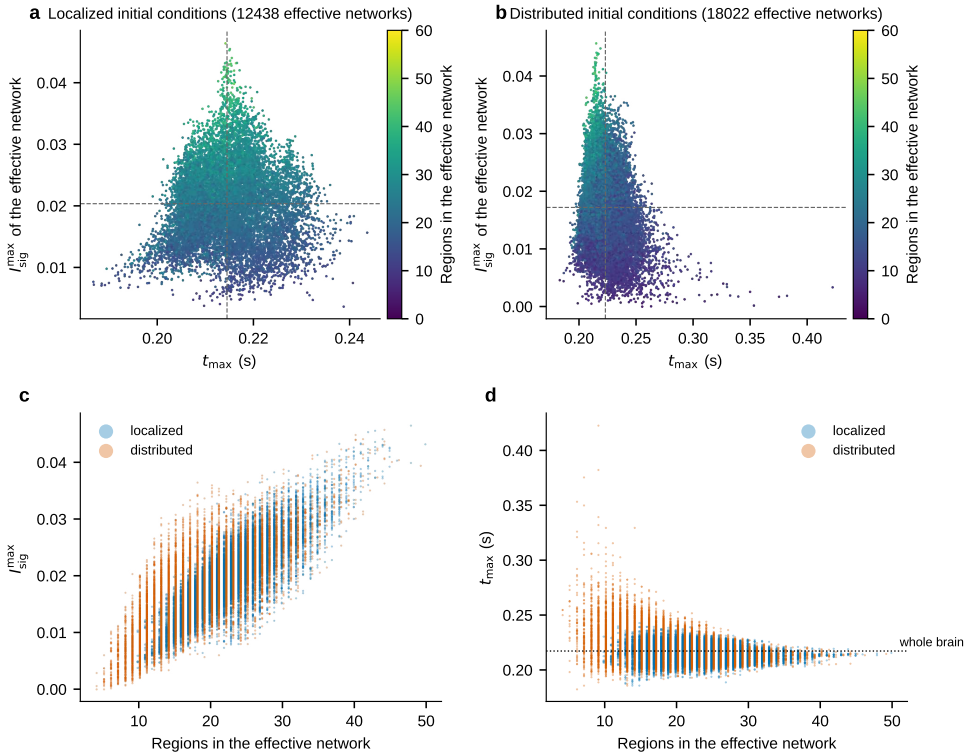


Fig. 4 Geometric richness of the effective networks. **a,b**, $I_{\text{sig}}^{\max}$ against $t_{\max}$ for the 12,438 networks of localized inputs (a) and the 18,022 networks of distributed inputs (b), coloured by the number of regions; dashed lines, means. **c**, $I_{\text{sig}}^{\max}$ against the number of regions. **d**, $t_{\max}$ against the number of regions; dashed line, $t_{\max}$ of the whole brain.

4.2 Effective networks along the axis of conscious states

In previous work on the human connectome (Estrada, 2026a) we showed that the conscious states can be placed along a single axis, the global coupling G of the coupling model. In that work, the couplings fitted to the functional connectivity of volunteers decreased by a median of 0.05 at loss of responsiveness under propofol and increased by a median of 0.14 under psilocybin. The reason why one parameter suffices is that the global coupling sets both the speed of propagation and the distance from the point at which the network-wide mode stops decaying. A natural question is therefore what happens to the ideas of the repertoire when the brain moves along this axis. To answer it, we recomputed the effective networks of the same 4,614 localized and 5,495 distributed inputs at couplings between 0.85 and 1.15, taking as t^* the time of maximal differentiation of the whole brain at each coupling (Fig. 5a,b).

From the awake coupling ($G = 0.963$) to that of loss of responsiveness ($G \approx 0.913$), the median effective network lost two regions for localized inputs (from 23 to 21) and

three for distributed inputs (from 18 to 15), and its median $I_{\mathrm{sig}}^{\max}$ fell by 17% and 20%, respectively. Under psilocybin ($G \approx 1.103$), in contrast, the networks gained six and eight regions and their median $I_{\mathrm{sig}}^{\max}$ rose by 52% and 73%. Meanwhile, the reading time changed little, from 0.221 s to 0.207 s. Ideas thus become poorer at loss of responsiveness and richer under psilocybin, in the same direction as the geometry of the whole brain (Estrada, 2026a). At every coupling, the number of different networks remained close to one per input (4,152–4,335 of 4,614 localized and 5,472–5,488 of 5,495 distributed inputs).

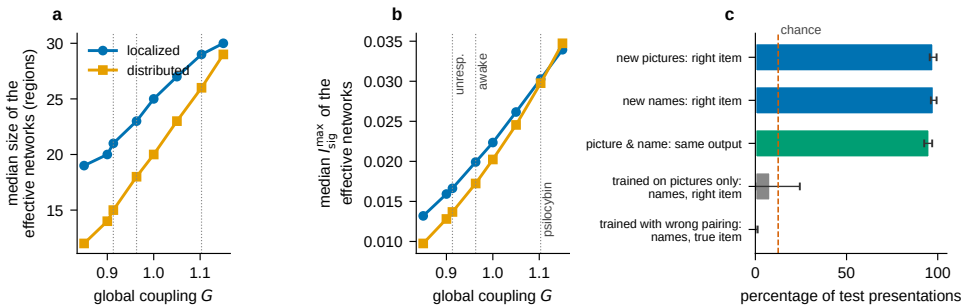


Fig. 5 Conscious states and inputs of different origin. **a,b**, Median size (a) and median $I_{\mathrm{sig}}^{\max}$ (b) of the effective networks of the same inputs along the global coupling; dotted lines, couplings of loss of responsiveness, awake state and psilocybin. **c**, Reader of the picture and the name of eight items (Hansen connectome; mean and range over ten seeds): correct item for new pictures and new names, same output for a picture and a name of the same item, and two controls; dashed line, chance.

4.3 Inputs of different origin and their association by the reader

We all recognize a person from a photograph and also from hearing her name. This is what happened in the experiments of Quian Quiroga and colleagues, in which one neuron of the human medial temporal lobe fired for different pictures of Jennifer Aniston, and another one fired both for pictures of Halle Berry and for her written name (Quian Quiroga et al., 2005, 2009). We therefore asked whether, in the model, inputs that enter through different systems, such as the picture and the name of the same person, produce the same effective network. With visual inputs on one to four regions of the visual network, 600 inputs gave 447 different effective networks, with a median of 20 regions, 13 of them visual. We then searched, over all nonnegative inputs of unit mass on a given set of starting regions, for one that reproduces a given network exactly, allowing every region of the network to cross the threshold at any of the 121 times of the grid up to t^* (Methods). From the visual regions the search reproduced all 447 networks, which validates it. From the control and default regions it proved, for all 447 networks, that no such input exists. From all non-visual regions it proved the same for 428 networks and reproduced 2, while 17 remained undecided within the time limit of the search. Forward simulation of about 41,000 inputs for each origin

(visual, non-visual, somatomotor, control and default) confirmed this picture. Each origin gave between 10,948 and 36,821 different effective networks, and no network was shared by two origins, for $\theta = 0.005$, 0.01, 0.02 and 0.05. The same result was obtained when the effective network was defined by the activity at t^* alone, in which case the only network shared at $\theta = 0.05$ was the empty one. In terms of Fig. 1, this is the situation of panel c: in all these tests the spoken word "red" and the picture of a red light selected different sets of regions.

The reason for this separation is structural. At t^* every region still keeps between 12% and 22% of its own initial activity (the diagonal of $P(t^*)$), so the regions where an input enters with enough mass always belong to its effective network, and within t^* the propagation reaches mainly their neighbours. An effective network therefore carries the regions through which its input entered. One could think that the separation would disappear if the hippocampus and the amygdala, where the cells of Quian Quiroga and colleagues were recorded, were part of the substrate. However, adding the hippocampus, amygdala, thalamus and striatum (HCP connectome of the ENIGMA toolbox with 14 subcortical regions (Larivière et al., 2021)) gave the same result for visual and auditory inputs, with no shared networks at any threshold and with both definitions. In this substrate 84% of the visual effective networks reached the hippocampus or the amygdala, which are directly connected to all visual regions but one, while no auditory network did, since the auditory regions are two connections away from them.

Since the picture and the name produce different effective networks, their common identity must be established by the reader. Let us imagine, for instance, that the DBM is presented with a picture of Halle Berry and with her spoken name. The two inputs select different networks, and the reader can only tell that they refer to the same person if it has learned to associate them. To test this, we built eight items, each with a picture (an input on its own visual region and up to three visual neighbours, with random amplitudes) and a name (an input on its own pair of auditory regions, sometimes with a third, with random amplitudes). Each item was presented 60 times as a picture and 60 times as a name, every presentation being a different input. The reader, a recurrent network of 200 units as in the DBM, received the activity of the regions of the effective network with noise and learned to output the item from 40 presentations of each kind; it was then tested on the other 20 (Methods). In all presentations, picture and name of the same item produced different effective networks, and their networks overlapped little, with an overlap (shared regions divided by regions in either) of 0.04 on the Hansen connectome. Nevertheless, the reader identified the item of 98% of the new pictures and of 98% of the new names, and it gave the same output to a picture and a name of the same item in 95% of the pairs, against 0.6% for different items (Fig. 5c). The subcortical substrate gave the same picture (98%, 97% and 96%). Two controls show that the identity is produced by the reader through learning. A reader trained on pictures only identified the item of 8% of the names, below the chance level of 12.5%, and a reader trained with the names paired with the wrong items assigned only 0.4% of the names to their true item. Just as a person identifies Halle Berry from her name only after having learned it together with her face, the association in the model is acquired.

We should note, however, that a reader that names an item can do so simply from which regions are active, using them as a label and ignoring the relations among them. Indeed, when the reader received only the active regions, each with a constant signal, it still gave the same output to picture and name in 86% of the pairs on the Hansen connectome (84% with the subcortical substrate), against 95% with the real activity. Identification is thus an observational task in the sense of GDT (Estrada, 2027, 2026a). The geometric level, by contrast, requires a reader that recovers the relations among the regions, and the reader used so far, a fixed random recurrent network whose final state is read out, keeps little of them. For 16 items with single-region pictures, the rank correlation between the true distances between items and the distances between the activities that reach the reader was 0.997, whereas the rank correlation between the true distances and the distances between the final states of the reader was only 0.18 (0.13 with the subcortical substrate). The geometric reader of GDT works differently, because it learns the propagation operator, from which the geometry of any set of regions follows (Estrada, 2026c). This is the reader that we examine next.

4.4 Reading the geometry of an effective network

For 200 effective networks of localized inputs (median 21.5 regions), a reader observed only the regions of the network, learned the propagation operator from their activity by linear regression (Methods), and predicted the geometry of the network at t^*. The response to the single input that created the network turned out to fix the geometry poorly: the rank correlation between the predicted and the true distances was 0.01 with the response observed up to t^*, and again 0.01 up to $4t^*$ (Fig. 6a). The ongoing, noise-driven activity of the same regions, in contrast, fixed it well, with rank correlations of 0.55 for one run of 43 s, 0.82 for 3.6 min and 0.95 for 14 min (0.57, 0.83 and 0.95 with 6% observation noise); observing the whole brain for 14 min gave 0.94. The reason is that a single response displays only one projection of the geometry, while ongoing activity explores the propagation in all directions, as anticipated for the DBM (Estrada, 2026c). In the example of Fig. 1, a single flash of the red light shows the reader only one view of the relations among the regions of its network, whereas the ongoing activity of the same regions shows all of them.

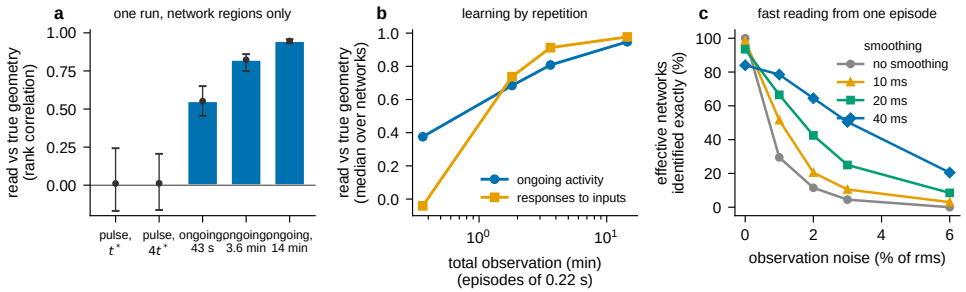


Fig. 6 Reading the geometry of effective networks. **a**, Rank correlation between the geometry read from the activity of the network's own regions and its true geometry, for the single response to its input and for ongoing activity observed for increasing times (median and 10th–90th percentiles over 200 networks). **b**, Learning by repetition: the reader learns the propagation of the whole substrate from many episodes of 0.22 s, of ongoing activity or of responses to localized inputs, and then reads the geometry of 200 new effective networks from their regions. **c**, Effective networks identified exactly by the reader from a single episode, against the observation noise, without and with smoothing of the observed activity.

We should clarify that the minutes required by a single run do not mean that every idea takes minutes to be read. They concern learning the propagation of the substrate, which is fixed by its anatomy and physiology, and therefore this propagation does not need to be learned anew for every idea. To show this, we let the reader learn the propagation of the whole substrate from many short episodes of 0.22 s, about t^*, and then asked it to read 200 new effective networks, never used in learning, from their regions alone. With episodes of ongoing activity, the rank correlation between read and true geometries was 0.38 after 100 episodes (0.4 min of total observation), 0.68 after 500, 0.81 after 1,000 and 0.95 after 4,000 (14.5 min). With episodes of responses to localized inputs it was 0.74 after 500, 0.91 after 1,000 and 0.98 after 4,000 (Fig. 6b). Repetitions of short episodes therefore teach the reader the propagation as well as one long run of the same total duration, and repeated short inputs teach it best. Once the propagation has been learned, reading an idea is immediate: the input selects the effective network, and the read geometry follows from its regions. In the context of the example in Fig. 1, this means that a reader that has met many lights, words and sounds before reads the red light as "red" as soon as its effective network is selected, and it reads it in the same way whichever of the many inputs that select this network has produced it.

To read the geometry, the reader must first identify the regions of the effective network from the activity of the single episode. Without observation noise it identified all 200 networks exactly. Observation noise, taken at its maximum over the episode, adds regions at the border of the network: with noise of 1%, 2%, 3% and 6% of the root-mean-square activity, 29.5%, 11.5%, 4.5% and 0% of the networks were identified exactly, with a median of 1, 3, 5 and 12 extra regions and no region missed (Fig. 6c). Fortunately, a simple smoothing of the observed activity over 40 ms before applying the threshold raised these fractions to 78.5%, 64.5%, 50.5% and 20.5%, with a median

of 0, 0, 0 and 1 extra regions. Without noise, smoothing lowers the peaks of the regions just above the threshold θ that defines the effective network, and 84% of the networks were then identified exactly. In every case, the read geometry of the identified regions agreed with their true geometry with a rank correlation of 0.976–0.977.

4.5 Effective networks in human stimulation data

So far, all effective networks have been computed in the model. Is there any experiment in which they can be observed in the human brain? Direct electrical stimulation of one cortical site, with recordings elsewhere, is the closest experimental counterpart of Definition 1, since it consists of one input and the regions that respond to it within a fraction of a second. The F-TRACT atlas gives, for pairs of parcels of the HCP-MMP1 parcellation (Glasser et al., 2016), the probability p_{ij} that stimulating parcel i evokes a significant cortico-cortical evoked potential in parcel j, estimated from 780 patients (David et al., 2013; Trebaul et al., 2018; Lemaréchal et al., 2022; F-TRACT consortium, 2021). We used the 26,771 pairs measured at least five times in patients older than 15 years, with 354 stimulated parcels. The model, unchanged, was run on the HCP structural connectome in the same parcellation (Larivière et al., 2021), with $t^* = 0.200$ s; the input was unit mass on the stimulated parcel, and the threshold was scaled to the number of parcels, $\theta = 0.01 \times 100/360$, which gives a median effective network of 40 parcels.

For every stimulated parcel with at least ten measured pairs (339 parcels), we compared the model effective network, restricted to the measured parcels, with the parcels that respond with $p_{ij} \geq 0.95$ (Fig. 7). Of the pairs inside the model effective networks, 67% responded with $p_{ij} \geq 0.95$, against 41% of the pairs outside and 50% of all measured pairs, an enrichment of 1.35. The Sørensen–Dice index (defined in Methods) between the model network and the responding parcels (Dice, 1945; Sørensen, 1948) had a median of 0.55, against 0.42 for random sets of the same size drawn from the measured parcels. The model was above the random sets in 323 of the 339 stimulated parcels, and above their 95th percentile in 194 (Wilcoxon signed-rank test, $p < 10^{-15}$). The real wiring is essential for this agreement: on a connectome rewired with the same number of connections per region, the networks spread to distant parcels, the enrichment fell to 0.98 and the Sørensen–Dice index to 0.12. The result holds for responders defined by $p_{ij} \geq 0.9$ and $p_{ij} \geq 0.99$ and for thresholds θ half and twice as large, with enrichments of 1.14–1.43 against 0.93–1.00 for the rewired connectome. Graded comparisons agree with this picture. The rank correlation between the peak activity of the model up to t^* and p_{ij} over all measured pairs was 0.27 (rewired connectome, -0.03), that with the amplitude of the evoked potentials was also 0.27, and the model separated the pairs with $p_{ij} \geq 0.9$ from the others with an area under the ROC curve of 0.68 (rewired, 0.50).

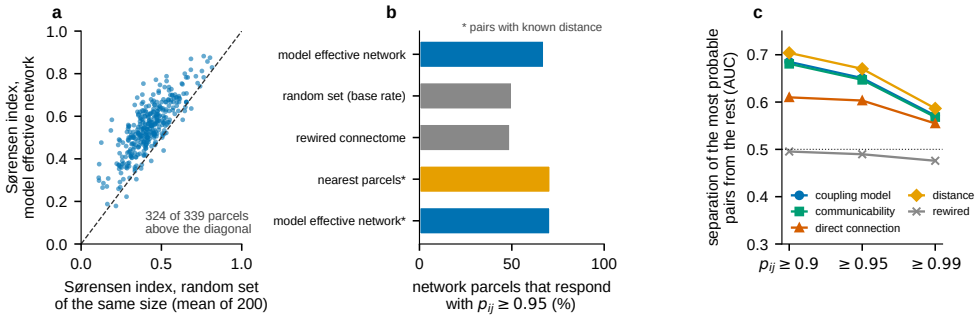


Fig. 7 Effective networks and human cortico-cortical evoked potentials (F-TRACT, HCP-MMP1, 339 stimulated parcels). **a**, Sørensen–Dice index between the model effective network of each stimulated parcel and the parcels that respond with $p_{ij} \geq 0.95$, against the mean index of 200 random sets of the same size drawn from the measured parcels. **b**, Fraction of the network parcels that respond with $p_{ij} \geq 0.95$, for the model, random sets (base rate), the rewired connectome and the nearest measured parcels (pairs with known Euclidean distance). **c**, Area under the ROC curve for separating the most probable pairs from the other measured pairs, for the coupling model and other predictors; dotted line, chance.

It is important to understand what this agreement means. In the 0.2 s of the reading time, activity has had time to travel only a short way from the stimulated parcel, both in the model and in the cortex, so that the model networks and the measured responses are both made of parcels close to the stimulated one. For this reason, sets of the same size made of the nearest measured parcels reproduced the responders as well as the model on the pairs with known distance (Sørensen–Dice index 0.63 for both). The same level of agreement was obtained with other connectome-based predictors, communicability (Estrada and Hatano, 2008) and shortest paths (rank correlations 0.26 and 0.25), because the connectome itself mostly links nearby parcels (Rubinov and Sporns, 2010). The agreement thus reflects how far the propagation on the human connectome reaches within the reading time, which is precisely what Definition 1 requires. Response latencies, which depend on axonal conduction delays absent from the coupling model, are outside its scope.

4.6 Two images at once: rivalry as serial reading

When each of the two eyes sees a different image, perception does not blend them: one image is seen while the other is suppressed, and the two alternate (Wheatstone, 1838; Levelt, 1965; Blake and Logothetis, 2002). Recordings of thousands of neurons in inferotemporal and prefrontal face patches of the macaque show that, during a stable percept, population activity alternates about 15 times per second between pure representations of the seen and of the suppressed face, both equally strong, with sharper feature tuning during the conscious epochs (Hesse et al., 2026). We asked first whether the dynamics of the substrate produces this alternation by itself. In the full nonlinear DMF (Deco et al., 2014), with feedback inhibition recalibrated at each coupling, we presented two sustained inputs, either on different visual regions or as

different patterns on the same 17 visual regions. In all 72 runs (four pairs of images, three input strengths, couplings 0.96, 1.5 and 2.0) they produced a stable mixture of the two patterns, never close to either pure pattern (Fig. 8a). This is because in the DMF every region has one excitatory population and inhibition acts within the region, so that two inputs simply add. Both images are therefore generated together, in agreement with the full representation of the suppressed image in the recordings (Hesse et al., 2026).

If the substrate does not select one of the images, the selection must take place in the reader. Suppose that what is read is one geometry at a time. Then a reader that has learned two items and receives the effective networks of both has no other option than to read them in turn. Such seriality has a clear advantage, since it avoids conflicting decisions. Think again of the traffic lights of Fig. 1d: a parallel reader would deliver "stop" and "go" at once for a red and a green light, whereas a serial reader delivers one of them at a time, just as action selection is serial in dual tasks (Pashler, 1994). We modelled the queue with the standard competition circuit of rivalry models, one output unit per learned item with mutual inhibition, adaptation and noise (Laing and Chow, 2002; Wilson, 2003), with time constants that give reading epochs of about 70 ms. The drive of each item was computed from GDT as the product of three factors: the overlap (Sørensen–Dice index) between the active network and the item's effective network, the item's $I_{\mathrm{sig}}^{\max}$, and the fidelity with which the reader reads its geometry. Fidelity depends on how often the item has been met. The reader learned each item from ten episodes of activity within its network per occurrence, and the median fidelity after 10, 20, 40, 80, 160 and 320 episodes was 0.15, 0.26, 0.47, 0.71, 0.85 and 0.94. The queue is thus weighted by the richness of each geometry and by its frequency.

For 300 pairs of distinct items drawn evenly across four classes of frequency (1, 2–3, 4–7 and at least 8), the reader alternated between the two items whenever their drives were within 30% of each other (92 of 92 pairs), with a median reading epoch of 63 ms (Fig. 8b,c). The weaker item was read 31%, 23% and 17% of the time for drive ratios 0.9–1.0, 0.8–0.9 and 0.7–0.8, and almost never below 0.7. Among pairs of equal frequency, the item with the richer geometry was read more in 94% of the pairs (31 pairs; Spearman correlation between the ratios of reading time and of $I_{\mathrm{sig}}^{\max}$, 0.96). Similarly, among pairs of similar richness ($I_{\mathrm{sig}}^{\max}$ within 15%), the more frequent item was read more in 98% (55 pairs; 0.96) (Fig. 8d). The two weights are independent in the repertoire, and in a joint regression of the log ratio of reading time they contributed with similar coefficients (3.2 for $I_{\mathrm{sig}}^{\max}$, 3.3 for fidelity and 3.5 for overlap). One important result is what happens when the union of the two networks is itself a learned item: in that case the reader read the union and neither component, and in 40 of 40 pairs the union was read more than the two components together. At the level of reading, compatible images are thus fused and incompatible ones are read in turn, as in perception (Blake and Logothetis, 2002), and familiar images are read longer, as upright faces dominate inverted ones (Engel, 1956). The reading epochs, of tens of milliseconds, are on the time scale of the alternation recorded during a stable percept (Hesse et al., 2026), whereas perceptual switches occur over seconds; fast serial reading is therefore a candidate mechanism, and its relation to perceptual switching is the natural next step.

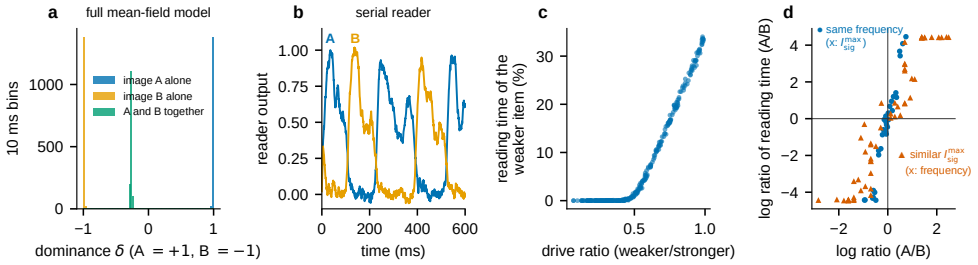


Fig. 8 Two images at once. **a**, Full nonlinear mean-field model with two input patterns on the same 17 visual regions: dominance δ in 10 ms bins (decomposition of the activity on the patterns of each image alone; +1, pure A; −1, pure B) for each image alone and for both together, which give a stable mixture. **b**, Outputs of the serial reader for two items with drive ratio 0.95. **c**, Reading time of the weaker item against the ratio of the drives, for 300 pairs. **d**, Log ratio of reading time against the log ratio of $I_{\text{sig}}^{\max}$ for pairs of equal frequency (blue circles) and against the log ratio of frequency for pairs of similar $I_{\text{sig}}^{\max}$ (vermilion triangles).

5 Discussion

The results obtained in this work answer the question of how a single anatomical network with a single dynamics can hold many ideas. Every input selects, at the reading time, the part of the substrate that its propagation reaches, and this effective network carries its own part of the geometry of the whole brain. Because the number of different effective networks grew almost in proportion to the number of inputs, the repertoire of a cortex of only 100 regions is far larger than the tens of thousands of networks that we sampled, which indeed means tens of thousands of potential ideas, and many more beyond our samples. The fact that the same network is reached from different inputs gives each idea a frequency, which is the natural counterpart of the familiarity of a content: a red light seen at dusk or at noon is still the same red light. The ideas also differ widely in geometric richness at equal size, and since richness is what distinguishes, in GDT, the geometries that can support conscious experience (Estrada, 2027), the repertoire contains ideas of very different experiential weight. Along the coupling axis on which functional connectivity places the conscious states (Estrada, 2026a), these ideas become poorer at loss of responsiveness and richer under psilocybin, coinciding with the experimental results which indicate that the complexity of the brain's responses collapses when consciousness is lost under anaesthesia (Casali et al., 2013) and that the diversity of spontaneous brain signals increases under psychedelics (Schartner et al., 2017; Carhart-Harris et al., 2014). The importance of this coincidence is that the variety and the richness of ideas follow the same parameter that sets the conscious state. In this way the model connects the level of consciousness, which is a property of the whole geometry, with its contents, which are the parts of that geometry selected by the inputs.

Additionally, the model tells us where the identity of a content is established. In all our simulations, inputs entering through different sensory systems produced different effective networks, and the reason is that at the reading time every region still

keeps a substantial part of its own initial activity. This is, in fact, the same property that makes the geometry most differentiated at $t_{\max}$, since a differentiated geometry requires responses that still remember where they started. The picture and the name of the same person are therefore two different effective networks, each with its own geometry, and their common identity has to be established by the reader, which associates both with the same item after learning them together. One idea thus corresponds to one effective network with its geometry, while the identity of a person or an object across pictures, words and sounds is a learned association between several such ideas. This interpretation agrees with what is known of the brain. For instance, it is known that imagery reactivates sensory cortex with patterns that overlap only partly with those of perception (Dijkstra et al., 2019), and that concept cells, which respond to the picture and to the name of the same person, lie in the medial temporal lobe, downstream of the sensory pathways, and acquire their responses through experience (Quian Quiroga et al., 2005, 2009; Quian Quiroga, 2012). Moreover, in the substrate that included subcortical structures, the visual effective networks reached the hippocampus and the amygdala within the reading time while the auditory ones did not. This suggests that the convergence of modalities in the medial temporal lobe takes place at the level of reading, after the effective networks have been formed, and not in the propagation itself.

It is natural to ask how this picture compares with the way in which other theories account for the contents of consciousness. The theories reviewed in the Introduction locate content in a cause–effect structure, as IIT does, in a broadcast representation, as the global workspace does, in a higher-order representation, or in the hypothesis of a generative model, as predictive processing does (Oizumi et al., 2014; Mashour et al., 2020; Brown et al., 2019; Hohwy and Seth, 2020). GDT with effective networks locates content in a part of the geometry generated by propagation on the anatomical network, and this choice has three consequences that can be computed. The first is that the repertoire of contents of a given substrate, and the frequency with which each content is reached, can be estimated from the connectome and the dynamics. The second is that the richness of each content can be measured, and that it changes in the expected direction with the conscious state. The third is that the identity of contents across modalities is explained by a mechanism, the learned association by the reader, which the model reproduces quantitatively. IIT shares with GDT the identification of content with a structure of relations, and its quality space corresponds here to the space of geometries of the effective networks, with the difference that the geometries of GDT can be computed on the human connectome. Additionally, predictive processing and higher-order theories share with the present model the idea that cross-modal identity is established at a level beyond the sensory pattern, the generative model or the higher-order representation, which corresponds here to the reader.

The tests of the reader also help us to see more clearly why GDT distinguishes two levels, observation and experience. Recognizing that a picture and a name refer to Halle Berry does not require the relations among the active regions, because the reader can use the set of active regions as a label, and indeed identification changed little when only the active regions were given to it. This is the observational level. Experiencing an idea, on the other hand, requires recovering the relations among its

regions, and the geometric reader of GDT does so by learning the propagation of the substrate, from which the geometry of any set of regions follows. Although this learning requires minutes of activity, it can be accumulated from many short episodes, in the spirit of learning by repetition (Hebb, 1949), and it concerns the substrate and not any particular idea. Once it has taken place, every effective network is read immediately, and the same network reached from different inputs is read as the same geometry. By contrast, a fixed random recurrent network, whose final state we read out, kept little of the relations between items, although these relations were present almost exactly in the activity that it received. Reading the geometry is therefore a property of readers that learn the propagation, which is the defining property of the DBM (Estrada, 2026c), and the relational structure of what such a reader reads can be measured with representational similarity analysis (Kriegeskorte et al., 2008).

Perhaps the most direct contact between the model and the human brain comes from electrical stimulation. The effective networks predicted on the human connectome overlap the parcels that respond to direct stimulation in 780 patients well above chance, and they do so only with the real wiring, since the agreement disappears on a rewired connectome with the same number of connections per region. Within the reading time both the model networks and the measured responses are local. This explains why the nearest parcels and other connectome-based predictors reach the same level of agreement, because structural connections link mostly nearby regions (Rubinov and Sporns, 2010). The level of agreement is therefore set by the connectome and by the sampling of the data, in which only implanted pairs are measured and half of them respond with probability at least 0.95. What the comparison establishes is that the reach of propagation on the human connectome within 0.2 s, which defines the effective network, matches the reach of evoked responses in the human cortex. The comparison thus supports the construction of effective networks by propagation, and the geometric account of conscious content is addressed by a more specific prediction. Electrical stimulation sometimes evokes an experience, such as a sensation, a movement or an emotion, while at many sites it evokes nothing (Penfield and Boldrey, 1937; Fox et al., 2020). The model makes a specific prediction for these observations: stimulation should evoke an experience when the effective network that it creates has a sufficiently rich geometry, with large $I_{\mathrm{sig}}^{\max}$ and appropriate $t_{\max}$.

On the other hand, the rivalry results place the selection of conscious content in the reader and not in the propagation. The substrate generates the effective networks of all inputs in parallel, as the full representation of the suppressed image in macaque cortex indicates (Hesse et al., 2026), and the reader reads one geometry at a time. A serial reader resolves incompatible inputs by reading them in turn, and the share of reading time that each input receives follows the richness of its geometry and its familiarity, that is, the frequency with which it has been met. At the level of reading, this principle reproduces several well-known properties of rivalry, namely the alternation itself, the dominance of stronger and of familiar images (Levelt, 1965; Engel, 1956), and the fusion of the two images when they form a learned whole. In this picture, the 15 Hz alternation recorded in face patches during a stable percept (Hesse et al., 2026) is a candidate for the reading cycle, with inferotemporal and prefrontal cortex taking part in reading; how this fast serial reading relates to perceptual switches, which occur

over seconds, is a question that the model now makes precise. Seriality also has a functional advantage, the avoidance of conflicting decisions, as in the case of the red and green traffic lights, which makes it a plausible product of evolution. The circuit that implements the queue, with its competition, adaptation and time scales, is the standard one of rivalry models (Laing and Chow, 2002; Wilson, 2003), and the specific contribution of GDT is the weights, which are computed from the geometry of each effective network and from the learning of the reader. As a consequence, the model predicts that the dominance of an image in rivalry grows with the geometric richness of its effective network at equal familiarity, and with its familiarity at equal richness.

In closing, it is worth situating these results within the range of validity of the model. The coupling model is the diffusion model derived from the DMF near its stationary state, and it therefore applies to perturbations that keep the dynamics in that regime. It has no axonal conduction delays, so response latencies, which depend on them (Lemaréchal et al., 2022), are outside its scope; what matters for the effective network is which regions are reached up to the reading time, not when they are reached. The threshold θ sets the size of the effective networks, and for this reason all results were obtained for several thresholds; on parcellations of different resolution, the threshold scales with the number of regions. Finally, the frequencies of the effective networks span about 1.3 decades in our samples, so the power law that fits them is an observation that larger samples will be able to test.

6 Methods

6.1 Connectomes

The main substrate is the group-consensus structural connectome of the Schaefer-100 parcellation of Hansen et al. (2022) (100 regions, 1136 connections), obtained from the public repository of that study; the matrix was symmetrized, its diagonal set to zero and its weights divided by the mean strength. The subcortical substrate is the HCP structural connectome of the ENIGMA toolbox for the Schaefer-100 parcellation with 14 subcortical regions (accumbens, amygdala, caudate, hippocampus, pallidum, putamen and thalamus of both hemispheres; 114 regions) (Larivière et al., 2021), and the substrate for the comparison with stimulation data is the HCP structural connectome of the same toolbox in the HCP-MMP1 parcellation (360 cortical parcels) (Glasser et al., 2016), reordered to the order of the F-TRACT parcels. Every substrate was normalized to unit mean strength and used with the same coupling model and parameters. The normalization fixes the units of G and does not act as a separate, small diffusion coefficient. For pure diffusion, multiplying all weights by a constant only rescales time; since the geometry is read at $t^* = t_{\max}$, which rescales with it, the effective networks are identical (on the Hansen connectome, with e^{-tL} and raw weights of mean strength 12.6, t^* is 12.6 times shorter, in the arbitrary time units of pure diffusion, than with normalized weights, $I_{\text{sig}}^{\max}$ is 1.048 in both cases, and the effective network is the same for all of 3,000 inputs). In the coupling model the weights enter only through GW, so raw weights with G divided by the mean strength give exactly the same generator, t^* and effective networks; raw weights with $G = 0.96$ would make the network-wide mode grow at 54 s^{-1}, far beyond the point $G_c = 1.19$ at which it

stops decaying. All times reported in this paper are in seconds of the coupling model, whose rates λ_0 and κ_0 come from the time constants of the DMF; they are therefore independent of the normalization. The coupling, and hence the effective diffusion coefficient, is fixed by the functional connectivity of the data (Estrada, 2026a), and its admissible range is bounded by the stability of the network. Network assignments follow the seven networks of the Schaefer parcellation (Schaefer et al., 2018); the visual network has 17 regions; the auditory regions are the six somatomotor parcels of the superior temporal and opercular cortex, with centroid $z < 20$ mm.

6.2 Coupling model and reading time

$M = \Lambda + \kappa L$ with $\Lambda_i = \lambda_0 - \kappa(1 - \vartheta)d_i$, $\kappa = \kappa_0 G$, $\lambda_0 = 5.952$ s^{-1}, $\kappa_0 = 7.287$ s^{-1}, $\vartheta = 0.357$ and $G = 0.96$ unless stated otherwise. $P(t) = e^{-tM}$ was computed from the eigendecomposition of the symmetric matrix M. The reading time t^* was obtained by bounded maximization of $I_{\mathrm{sig}}(t)$ of the whole substrate over $\log t$ between 10^{-3} and 30 s: 0.217 s (Hansen, $G = 0.96$), 0.218 s (HCP cortex), 0.211 s (HCP with subcortex) and 0.200 s (HCP-MMP1). The slowest mode of M decays at 1.16 s^{-1} on the Hansen connectome, a relaxation time of 0.86 s.

6.3 Inputs and effective networks

Localized inputs were built by choosing a region at random and up to three of its neighbours (number chosen uniformly from 0 to 3), with amplitudes uniform in $[0.1, 1.1]$; distributed inputs by choosing 1 to 10 regions at random anywhere, with the same amplitudes. All inputs were normalized to unit mass, and identical inputs (after rounding to 10^{-12}) were removed. Of 20,000 sampled inputs of each family, 15,073 localized and 18,105 distributed were different. The maximum of $x_i(s)$ over $[0, t^*]$ was evaluated on 61 equally spaced times for the repertoire and on 121 for all other analyses. For the coupling axis, the same 4,614 localized and 5,495 distributed inputs (from 6,000 sampled of each family) were used at $G = 0.85$, 0.90, 0.913, 0.963, 1.00, 1.05, 1.103 and 1.15. The reference couplings are the median awake coupling of the propofol volunteers (0.963), and this value minus 0.05 and plus 0.14, the median changes at loss of responsiveness and under psilocybin (Estrada, 2026a).

6.4 Geometry of the effective networks

$I_{\mathrm{sig}}^{(e)}(t)$ was computed from the distances $D(t)$ of the whole substrate restricted to the regions of each network, on 90 logarithmically spaced times between 10^{-3} and 30 s, and its maximum was refined by fitting a parabola in $\log t$ to the grid maximum and its two neighbours. Networks with fewer than three regions were excluded from the statistics of richness.

6.5 Frequencies

The frequency of a network is the number of different inputs that produce it. The distribution of frequencies was fitted with discrete power-law, exponential and truncated power-law distributions by maximum likelihood, and the fits were compared by normalized likelihood-ratio tests (Clauset et al., 2009; Vuong, 1989).

6.6 Inputs of different origin

For the exact search, 600 visual inputs (one to four visual regions, amplitudes uniform in $[0.1, 1.1]$, unit mass) defined the perceived networks. For each network E and set of starting regions S, we asked whether some $\boldsymbol{u} \geq 0$ supported on S with $\sum_i u_i = 1$ satisfies $(P(s_k)\boldsymbol{u})_j \leq \theta(1 - 10^{-3})$ for every region $j \notin E$ at all 121 times s_k of $[0, t^*]$, and, for every $i \in E$, $(P(s_k)\boldsymbol{u})_i \geq \theta(1 + 10^{-3})$ at some time s_k of the same grid. The existence of a crossing time was written as a mixed-integer program with one binary variable per region of E and grid time (HiGHS). Before it, a necessary condition was tested for every region $i \in E$: a linear program maximized the activity of i over the inputs that keep all regions outside E below the threshold, with the coefficients of a set of grid times replaced by their elementwise maximum, an upper bound because the inputs are nonnegative; a set was split only when its bound reached the threshold, and a region that cannot reach it at any grid time proves that E cannot be reproduced. Networks that passed this test were given to the mixed-integer program, with a limit of 300 s, after a linear program at the reading time or at the peak time under the visual input. Every solution was verified by forward simulation. For the shared repertoire, 50,000 inputs were sampled for each origin (half localized, with neighbours of the same origin, half distributed within the origin), of which about 41,000 were different, and the effective networks were compared exactly.

6.7 Reader of items

Eight items were assigned at random a visual region and a pair of auditory regions (ten seeds). A picture was an input on the visual region and up to three visual neighbours, with amplitudes $0.15 + U(0, 1)$ and 0.9 added to the first region; a name was an input on the pair of auditory regions, with probability 0.5 also on a third auditory region, with amplitudes $0.15 + U(0, 1)$ and 0.9 added to the pair. Every item was presented 60 times as a picture and 60 times as a name. The reader received the activity of the regions of the effective network of each presentation ($\theta = 0.01$, rule "is or has been") at 24 logarithmically spaced times between $t^*/10$ and t^*, with zero activity on the other regions and additive Gaussian noise of 0.06 times the root-mean-square activity. The reader is the leaky recurrent network $\boldsymbol{m}_{k+1} = (1-a)\boldsymbol{m}_k + a \tanh(W\boldsymbol{m}_k + W_{\text{in}}\boldsymbol{x}(\tau_k) + \boldsymbol{c})$ with 200 units, $a = 0.35$, sparse random recurrent weights (density 0.10) scaled to spectral radius 0.88, input weights uniform in $[-0.65, 0.65]/\sqrt{n}$ and biases uniform in $[-0.15, 0.15]$; its final state was read by a linear readout onto the one-hot code of the item, fitted by ridge regression (parameter 10^{-4}) on 40 presentations of each kind and tested on the other 20. In the regions-only control, every active region received a constant signal equal to the root-mean-square of the nonzero activities. For the relations between items, 16 items with pictures on a single visual region and 60 noisy

presentations each were used, and the distances between the mean activities and between the mean final states of the reader were compared with $D(t^*)$ between the regions of the items by Spearman rank correlation.

6.8 Learning the propagation

The reader estimated a one-step operator A by least squares from the observed activity, $\boldsymbol{x}_{k+1} = A\boldsymbol{x}_k$, and the generator $\widetilde{M} = -\log(A)/\Delta t$ (principal matrix logarithm, real part); the read geometry is that of $e^{-t^*\widetilde{M}}$. For the single response, the response to the input of the network was observed on its regions at 241 equally spaced times up to t^* or $4t^*$, with 6% observation noise. Ongoing activity was simulated for the whole substrate with the exact discretization $\boldsymbol{x}_{k+1} = e^{-M\Delta t}\boldsymbol{x}_k + \boldsymbol{\eta}_k$, $\Delta t = 5$ ms, with Gaussian $\boldsymbol{\eta}_k$ of covariance $\int_0^{\Delta t} e^{-2Ms}ds$, for 50, 250 and 1000 relaxation times of the slowest mode, and observed on the regions of each network. For learning by repetition, episodes of 43 steps of 5 ms ($\approx t^*$) were either ongoing activity started from the stationary distribution or responses to random localized inputs with 6% observation noise; all transitions of all episodes were pooled in the regression. The 200 test networks came from new localized inputs. For identification, the reader thresholded at θ the maximum over the episode of the observed activity of every region, with observation noise of 0, 1, 2, 3 and 6% of the root-mean-square activity, without smoothing or after a moving average over 10, 20 or 40 ms. The score is the Spearman rank correlation between read and true distances over the pairs of regions of each network.

6.9 Comparison with stimulation data

F-TRACT atlas v2112 (F-TRACT consortium, 2021), patients older than 15 years, HCP-MMP1 parcellation: probability of a significant response, peak latency and amplitude for every pair of stimulated and recorded parcels, with values reported for pairs measured at least five times. For each stimulated parcel the model input was unit mass on that parcel, and the peak activity of every parcel over 241 times up to t^* defined the effective network ($\theta = 0.01 \times 100/360$; also half and twice this value). Responders were the measured parcels with $p_{ij} \geq c$, $c = 0.9$, 0.95 or 0.99. For each stimulated parcel with at least ten measured pairs, the effective network was restricted to the measured parcels and compared with the responders by the fraction of network parcels that respond, the fraction of responders inside the network and the Sørensen–Dice index $2|A \cap B|/(|A| + |B|)$; random sets of the same size were drawn 200 times from the measured parcels. The rewired connectomes were obtained by degree-preserving double-edge swaps (five swaps per edge, weights carried by the edges; five realizations). The nearest-parcel sets contained, for each stimulated parcel, as many measured parcels as the model network, chosen by the Euclidean distance given by F-TRACT (15,772 pairs). Communicability was $e^{W/\lambda_{\max}}$ and the shortest path was computed with lengths $-\log(W_{ij}/\max W)$. Areas under the ROC curve were computed over all measured pairs.

6.10 Rivalry

Full DMF (Deco et al., 2014): $I_{E,i} = W_E I_0 + w_+ J_{\mathrm{NMDA}} S_{E,i} + G J_{\mathrm{NMDA}} \sum_j C_{ij} S_{E,j} - J_i S_{I,i} + I_{\mathrm{ext},i}$, $I_{I,i} = W_I I_0 + J_{\mathrm{NMDA}} S_{E,i} - S_{I,i}$, $\dot{S}_{E,i} = -S_{E,i}/\tau_E + (1 - S_{E,i}) \gamma H_E(I_{E,i}) + \sigma \nu_i$, $\dot{S}_{I,i} = -S_{I,i}/\tau_I + H_I(I_{I,i}) + \sigma \nu'_i$, with $H(I) = (aI - b)/(1 - e^{-d(aI-b)})$, $a_E = 310$ nC^{-1}, $b_E = 125$ Hz, $d_E = 0.16$ s, $a_I = 615$ nC^{-1}, $b_I = 177$ Hz, $d_I = 0.087$ s, $\tau_E = 0.1$ s, $\tau_I = 0.01$ s, $\gamma = 0.641$, $I_0 = 0.382$ nA, $W_E = 1$, $W_I = 0.7$, $w_+ = 1.4$, $J_{\mathrm{NMDA}} = 0.15$ nA and $\sigma = 0.01$ nA; the inhibitory couplings J_i were set by feedback inhibition control so that every region fires at 3.06 Hz. Integration by Euler–Maruyama with step 0.1 ms, 20 s per run, the first 6 s discarded. Images were sustained inputs of 0.02–0.1 nA on a visual region and two visual neighbours, or of 0.01–0.05 nA distributed over the 17 visual regions with random graded patterns. The activity in 10 ms bins, minus the baseline, was decomposed by least squares on the mean patterns of each image alone, α and β, and $\delta = (\alpha - \beta)/(|\alpha| + |\beta|)$. Serial reader: items were effective networks of 12–30 regions from localized inputs (up to 60 per class of frequency). The fidelity of an item after n learning episodes (responses to localized inputs within its network, observed on its regions with 6% noise, operator learned as above) was measured on 40 items with three repetitions and fitted by $f(n) = 1 - \exp[-(n/n_0)^b]$, $n_0 = 70$, $b = 0.87$; an item of frequency ϕ has $n = 10\phi$. With two items present, the active network is the effective network of the sum of their inputs, and the drive of item k is $\mathrm{Dice}(V_{\mathrm{active}}, V_k)\, I_{\mathrm{sig}}^{\max}(k)\, f(n_k)$, normalized by the larger drive. The queue is $\tau \dot{y}_k = -y_k + S(d_k - \beta \sum_{l \neq k} y_l - g a_k) + \eta_k$, $\tau_a \dot{a}_k = -a_k + y_k$, with $S(x) = 1/(1 + e^{-(x-0.3)/0.08})$, $\tau = 10$ ms, $\tau_a = 80$ ms, $\beta = 2$, $g = 1.5$ and noise of amplitude 0.05; an item is read when its unit exceeds 0.5 and the other by at least 0.3; 20 s per pair. For fusion, the union network was added as a third item with 100 learning episodes.

6.11 Statistics and software

Rank correlations are Spearman correlations; paired comparisons across stimulated parcels used Wilcoxon signed-rank tests and pooled enrichments a one-sided binomial test. All analyses were carried out with custom scripts in Python (NumPy, SciPy, scikit-learn); MATLAB codes that reproduce them are provided as Online Resource 2. The parameters of all models, the results for every threshold, substrate and setting, and the list of codes are given in Online Resource 1.

6.12 Use of large language models

Claude (Anthropic) was used to assist in writing and running the computational scripts and in drafting and editing the manuscript. The author designed the study, checked the code and all results, reviewed and edited all the text, and takes full responsibility for the content of the paper.

7 Conclusions

Effective networks give Geometro-Diffusion Theory a mechanism by which one brain substrate with one dynamics generates many ideas. Every input selects, at the time

at which the geometry is read, a part of the substrate that carries its own part of the brain's geometry. The repertoire of these networks is very large, the same network is reached from different inputs, and the networks differ widely in geometric richness, which decreases at loss of responsiveness and increases under psilocybin along the coupling axis of the conscious states. Inputs entering through different senses produce different networks, whose common identity is established by a reader through learning, and a reader that learns the propagation of the substrate by repetition reads the geometry of every effective network immediately. When two images are present, both networks are generated and a serial reader reads them in turn, weighted by their richness and familiarity, which places the selection of conscious content in reading. The effective networks predicted on the human connectome match the reach of evoked responses in the human cortex. Together, these results connect one brain geometry with the many ideas that it holds, and they lead to quantitative predictions for stimulation experiments that relate the richness of an effective network to the experience it evokes.

Supplementary information

Online Resource 1 (Supplementary Material_JCompNeuro.pdf) contains the parameters of all models, the results for every threshold, substrate and setting summarized in the text, and the list of codes. Online Resource 2 (ESM_2_JCompNeuro.zip) contains the MATLAB codes that reproduce all results.

Declarations

- **Funding.** This work was supported by Agencia Estatal de Investigación (AEI, MCI, Spain) MCIN/AEI/10.13039/501100011033 under grant PID2023-149473NB-I00 and by Agencia Estatal de Investigación (AEI, MCI, Spain) MCIN/AEI/10.13039/501100011033 and Fondo Europeo de Desarrollo Regional (FEDER, UE) under the María de Maeztu Program for units of Excellence in R&D, grant CEX2021-001164-M.

- **Competing interests.** The author declares no competing interests.
- **Ethics approval and consent to participate.** Not applicable. The study uses only publicly available, anonymized group-level data: structural connectomes (Hansen et al., 2022; Larivière et al., 2021) and the F-TRACT atlas (F-TRACT consortium, 2021).
- **Consent for publication.** Not applicable.
- **Data availability.** The Hansen connectome is available from the repository of Hansen et al. (2022), the HCP connectomes from the ENIGMA toolbox (Larivière et al., 2021), and the F-TRACT atlas from Zenodo (F-TRACT consortium, 2021).
- **Code availability.** The MATLAB codes that reproduce all results, and the model parameters, are freely available for academic use as Online Resource 2.
- **Author contributions.** E.E. conceived the study, developed the theoretical framework, designed and performed the calculations, analysed the results, and wrote the manuscript.

References

Blake, R., Logothetis, N.K.: Visual competition. Nat Rev Neurosci **3**, 13–21 (2002)

Brown, R., Lau, H., LeDoux, J.E.: Understanding the higher-order approach to consciousness. Trends in Cognitive Sciences **23**(9), 754–768 (2019) https://doi.org/10.1016/j.tics.2019.06.009

Casali, A.G., Gosseries, O., Rosanova, M., Boly, M., Sarasso, S., Casali, K.R., Casarotto, S., Bruno, M.-A., Laureys, S., Tononi, G., Massimini, M.: A theoretically based index of consciousness independent of sensory processing and behavior. Sci Transl Med **5**(198), 198–105 (2013)

Carhart-Harris, R.L., Leech, R., Hellyer, P.J., Shanahan, M., Feilding, A., Tagliazucchi, E., Chialvo, D.R., Nutt, D.: The entropic brain: a theory of conscious states informed by neuroimaging research with psychedelic drugs. Frontiers in Human Neuroscience **8**, 20 (2014)

Coifman, R.R., Lafon, S.: Diffusion maps. Appl Comput Harmon Anal **21**, 5–30 (2006)

Clauset, A., Shalizi, C.R., Newman, M.E.J.: Power-law distributions in empirical data. SIAM Rev **51**, 661–703 (2009)

Dijkstra, N., Bosch, S.E., Gerven, M.A.J.: Shared neural mechanisms of visual perception and imagery. Trends Cogn Sci **23**, 423–434 (2019)

Dehaene, S., Changeux, J.-P.: Experimental and theoretical approaches to conscious processing. Neuron **70**(2), 200–227 (2011) https://doi.org/10.1016/j.neuron.2011.03.018

Dice, L.R.: Measures of the amount of ecologic association between species. Ecology **26**, 297–302 (1945)

David, O., Job, A.-S., De Palma, L., Hoffmann, D., Minotti, L., Kahane, P.: Probabilistic functional tractography of the human cortex. NeuroImage **80**, 307–317 (2013)

Deco, G., Kringelbach, M.L., Jirsa, V.K., Ritter, P.: The dynamics of resting fluctuations in the brain: metastability and its dynamical cortical core. Sci Rep **7**, 3095 (2017)

Deco, G., Ponce-Alvarez, A., Hagmann, P., Romani, G.L., Mantini, D., Corbetta, M.: How local excitation-inhibition ratio impacts the whole brain dynamics. Journal of Neuroscience **34**, 7886–7898 (2014)

Estrada, E., Hatano, N.: Communicability in complex networks. Phys Rev E **77**, 036111 (2008)

Engel, E.: The role of content in binocular resolution. Am J Psychol **69**, 87–91 (1956)

Estrada, E.: Brain diffusion geometry reflects conscious states under magnetic stimulation, anaesthesia and psychedelics. Submitted (2026)

Estrada, E.: Can qualia be geometric? Geometro-Diffusion Theory and the structure of conscious experience. Cogn Neurodyn (in press) (2026)

Estrada, E.: Geometro-Diffusion Theory of consciousness. The diffusion-based machine. Theory Biosci (in press) (2026)

Estrada, E.: Loss of consciousness as a collapse of neural propagation geometry. A Geometro-Diffusion Theory approach. Chaos Solitons Fractals **213**, 119283 (2026)

Estrada, E.: From neural propagation to conscious experience: A geometro-diffusion theory of consciousness. J Theor Biol **636**, 112610 (2027)

F-TRACT consortium: F-TRACT atlas, version v2112. Zenodo, https://zenodo.org/records/7015414 (2021)

Friston, K.: Am i self-conscious? (or does self-organization entail self-consciousness?). Frontiers in Psychology **9**, 579 (2018) https://doi.org/10.3389/fpsyg.2018.00579

Fox, K.C.R., Shi, L., Baek, S., Raccah, O., Foster, B.L., Saha, S., *et al.*: Intrinsic network architecture predicts the effects elicited by intracranial electrical stimulation of the human brain. Nat Hum Behav **4**, 1039–1052 (2020)

Glasser, M.F., Coalson, T.S., Robinson, E.C., Hacker, C.D., Harwell, J., Yacoub, E., *et al.*: A multi-modal parcellation of human cerebral cortex. Nature **536**, 171–178 (2016)

Hansen, J.Y., *et al.*: Mapping neurotransmitter systems to the structural and functional organization of the human neocortex. Nat Neurosci **25**, 1569–1581 (2022)

Hebb, D.O.: The Organization of Behavior. Wiley, New York (1949)

Haxby, J.V., Gobbini, M.I., Furey, M.L., Ishai, A., Schouten, J.L., Pietrini, P.: Distributed and overlapping representations of faces and objects in ventral temporal cortex. Science **293**, 2425–2430 (2001)

Hesse, J.K., Lanfranchi, F.F., McGrory, C., Shi, Y., Engel, T.A., Tsao, D.Y.: Rapid alternation of conscious and suppressed stimulus representations in the primate brain. bioRxiv preprint, doi:10.64898/2026.10.15.759299 (2026)

Haynes, J.-D., Rees, G.: Decoding mental states from brain activity in humans. Nat Rev Neurosci **7**, 523–534 (2006)

Hohwy, J., Seth, A.K.: Predictive processing as a systematic basis for identifying the

neural correlates of consciousness. Philosophy and the Mind Sciences **1**(II) (2020) https://doi.org/10.33735/phimisci.2020.II.64

Kriegeskorte, N., Mur, M., Bandettini, P.: Representational similarity analysis – connecting the branches of systems neuroscience. Front Syst Neurosci **2**, 4 (2008)

Kleiner, J., Tull, S.: The mathematical structure of integrated information theory. Front Appl Math Stat **6**, 602973 (2021)

Lamme, V.A.F.: Towards a true neural stance on consciousness. Trends in Cognitive Sciences **10**(11), 494–501 (2006) https://doi.org/10.1016/j.tics.2006.09.001

Laing, C.R., Chow, C.C.: A spiking neuron model for binocular rivalry. J Comput Neurosci **12**, 39–53 (2002)

Levelt, W.J.M.: On Binocular Rivalry. Institute for Perception RVO-TNO, Soesterberg (1965)

Lemaréchal, J.-D., Jedynak, M., Trebaul, L., Boyer, A., Tadel, F., *et al.*: A brain atlas of axonal and synaptic delays based on modelling of cortico-cortical evoked potentials. Brain **145**, 1653–1667 (2022)

Larivière, S., Paquola, C., Park, B.-y., Royer, J., Wang, Y., Benkarim, O., *et al.*: The ENIGMA Toolbox: multiscale neural contextualization of multisite neuroimaging datasets. Nat Methods **18**, 698–700 (2021)

Mashour, G.A., Roelfsema, P., Changeux, J.-P., Dehaene, S.: Conscious processing and the global neuronal workspace hypothesis. Neuron **105**, 776–798 (2020)

Oizumi, M., Albantakis, L., Tononi, G.: From the phenomenology to the mechanisms of consciousness: Integrated information theory 3.0. PLoS Computational Biology **10**(5), 1003588 (2014) https://doi.org/10.1371/journal.pcbi.1003588

Pashler, H.: Dual-task interference in simple tasks: data and theory. Psychol Bull **116**, 220–244 (1994)

Penfield, W., Boldrey, E.: Somatic motor and sensory representation in the cerebral cortex of man as studied by electrical stimulation. Brain **60**, 389–443 (1937)

Quian Quiroga, R.: Concept cells: the building blocks of declarative memory functions. Nat Rev Neurosci **13**, 587–597 (2012)

Quian Quiroga, R., Kraskov, A., Koch, C., Fried, I.: Explicit encoding of multimodal percepts by single neurons in the human brain. Curr Biol **19**, 1308–1313 (2009)

Quian Quiroga, R., Reddy, L., Kreiman, G., Koch, C., Fried, I.: Invariant visual representation by single neurons in the human brain. Nature **435**, 1102–1107 (2005)

Rubinov, M., Sporns, O.: Complex network measures of brain connectivity: uses and interpretations. Neuroimage **52**, 1059–1069 (2010)

Seth, A.K., Bayne, T.: Theories of consciousness. Nat Rev Neurosci **23**, 439–452 (2022)

Schartner, M.M., Carhart-Harris, R.L., Barrett, A.B., Seth, A.K., Muthukumaraswamy, S.D.: Increased spontaneous MEG signal diversity for psychoactive doses of ketamine, LSD and psilocybin. Sci Rep **7**, 46421 (2017)

Shanahan, M.: Metastable chimera states in community-structured oscillator networks. Chaos **20**(1), 013108 (2010)

Storm, J.F., Klink, P.C., Aru, J., Senn, W., Goebel, R., *et al.*: An integrative, multiscale view on neural theories of consciousness. Neuron **112**, 1531–1552 (2024) https://doi.org/10.1016/j.neuron.2024.02.004

Schaefer, A., Kong, R., Gordon, E.M., Laumann, T.O., Zuo, X.-N., Holmes, A.J., Eickhoff, S.B., Yeo, B.T.T.: Local-global parcellation of the human cerebral cortex from intrinsic functional connectivity MRI. Cereb Cortex **28**, 3095–3114 (2018)

Sørensen, T.: A method of establishing groups of equal amplitude in plant sociology based on similarity of species content. Biol Skr **5**, 1–34 (1948)

Tononi, G., Albantakis, L., Barbosa, L., Boly, M., Cirelli, C., *et al.*: Consciousness or pseudo-consciousness? A clash of two paradigms. Nat Neurosci **28**, 694–702 (2025) https://doi.org/10.1038/s41593-025-01880-y

Tononi, G., Boly, M., Massimini, M., Koch, C.: Integrated information theory: from consciousness to its physical substrate. Nat Rev Neurosci **17**, 450–461 (2016)

Trebaul, L., Deman, P., Tuyisenge, V., Jedynak, M., Hugues, E., Rudrauf, D., *et al.*: Probabilistic functional tractography of the human cortex revisited. NeuroImage **181**, 414–429 (2018)

Vuong, Q.H.: Likelihood ratio tests for model selection and non-nested hypotheses. Econometrica **57**, 307–333 (1989)

Wheatstone, C.: Contributions to the physiology of vision. Part the first. On some remarkable, and hitherto unobserved, phenomena of binocular vision. Phil Trans R Soc Lond **128**, 371–394 (1838)

Wilson, H.R.: Computational evidence for a rivalry hierarchy in vision. Proc Natl Acad Sci USA **100**, 14499–14503 (2003)

Wong, K.-F., Wang, X.-J.: A recurrent network mechanism of time integration in perceptual decisions. Journal of Neuroscience **26**, 1314–1328 (2006)

Supplementary Files

This is a list of supplementary files associated with this preprint. Click to download.

- SupplementaryMaterialJCompNeuro.pdf
- ESM2JCompNeuro.zip